Anticancer Complexes

Effects of Terminal Substitution and Iron Coordination on Antiproliferative Activity of L-Proline-salicylaldehyde–Thiosemicarbazone Hybrids

Miljan N. M. Milunović*[a,d] Aliona Dobrova,[a] Ghenadie Novitchi,[b] Nevenka Gligorijević,[c] Siniša Radulović,[c] Jozef Kožíšek,[d] Peter Rapta,[d] Eva A. Enyedy,[e] and Vladimir B. Arion*[a]

Abstract: A series of five iron(III) complexes, namely [Fe(**HL¹**)Cl₂] (**1**), [Fe(**HL²**)Cl₂]·1.6H₂O (**2**·1.6H₂O), [Fe(**HL³**)(MeOH)Cl₂]·0.5H₂O (**3**·0.5H₂O), [Fe(**HL⁴**)(MeOH)Cl₂]·0.5H₂O (**4**·0.5H₂O) and [Fe(**HL⁴**)(DMF)Cl₂]·0.5Et₂O·H₂O (**4′**·0.5Et₂O·H₂O), where **H₂L¹** = L-proline-salicylaldehyde–thiosemicarbazone (L-Pro-STSC), **H₂L²** = pyrrolidine-substituted L-Pro-STSC, **H₂L³** = phenyl-substituted L-Pro-STSC, and **H₂L⁴** = naphthyl-substituted L-Pro-STSC, have been synthesized. The two ligand precursors (**H₂L³** and **H₂L⁴**) and iron complexes were characterized by elemental analysis, spectroscopic methods (UV/Vis, IR, and NMR), ESI mass spectrometry, cyclic voltammetry, and single-crystal X-ray crystallography (**1–3** and **4′**). Magnetic properties of the five-coordinate complex **2** and six-coordinate complex **4** have also been investigated. The antiproliferative activity of the or-

ganic hybrids and their iron(III) complexes have been studied in vitro in five human cell lines and one murine cancer cell line, namely HeLa (cervical cancer), FemX (melanoma), A549 (alveolar basal adenocarcinoma), LS-174 (colon cancer), MDA-MB-453 (breast cancer) and MS1 (transformed murine endothelial), as well as in human noncancerous fetal lung fibroblast cell line (MRC-5). According to the structure–activity relationship, introduction of aromatic groups such as phenyl or naphthyl enhances the cytotoxic potency of the hybrids in the following order **H₂L¹** < **H₂L²** < **H₂L³** < **H₂L⁴**. Coordination of the hybrids to iron(III) improves their antiproliferative activity in the majority of investigated cell lines with exception of **H₂L³** in LS-174, **H₂L⁴** in MS1, and both **H₂L³** and **H₂L⁴** in FemX cell lines, where an opposite effect was observed.

Introduction

Thiosemicarbazones (TSCs) as excellent metal chelators are a class of organic compounds with structural diversity[1,2] and broad spectrum of pharmacological activities, such as antiproliferative, antiviral, antibacterial, antimalarial, and antifungal.[3] The research interest in TSCs as antiproliferative agents was aroused in the 1950's, when p-aminobenzaldehyde thiosemicarbazone was found to inhibit virus multiplication, where the synthesis of nucleoproteins was required.[4] Later on, by replacement of the benzaldehyde moiety with pyridine-2-carbox-

aldehyde one, two new compounds, namely 5-hydroxy-2-formylpyridine thiosemicarbazone (5-HP)[5,6] and 3-aminopyridine-2-carboxaldehyde thiosemicarbazone (Triapine),[7] were discovered to possess much higher anticancer activity in vitro and in vivo compared to 2-hydroxy-benzaldehyde thiosemicarbazones and were promoted to clinical studies. The reason for this cytotoxicity enhancement is still unknown. Triapine was investigated in more than 20 clinical phase I and II trials as an anticancer drug candidate, showing mixed results and considerable side effects.[8] However, it still remains a prominent investigational TSC in the fight against cancer.

Two enzymes, namely ribonucleotide reductase (RNR)[9] and topoisomerase II (topo II), which are responsible for DNA synthesis and (de)catenation of the DNA chain during transcription, as well as replication and repair, are predominantly studied as targets for the elucidation of the underlying mechanisms of their antiproliferative activity. It is well known that disturbance of the enzyme activity (RNR and/or topo II) indirectly leads to cell apoptosis.[10] Other events such as mitochondrial disruption,[11] inhibition of multidrug resistance protein,[12] inhibition of epithelial-to-mesenchymal transition,[13] and inhibition of oncogenic signaling pathways[14] are also attributed to the anticancer activity of TSCs.

Drug design strategies for the enhancement of the cytotoxicity of TSCs rely on the introduction of either bulky aliphatic and aromatic groups or a heteroatom in the TSC backbone, as well as on metal coordination.[2,8,15–18]

[a] *Institute of Inorganic Chemistry, University of Vienna, Faculty of Chemistry, Währinger Strasse 42, 1090, Austria*
E-mail: miljan.milunovic@univie.ac.at
          vladimir.arion@univie.ac.at
http://anorg-chemie.univie.ac.at/magnoliaPublic/Research/Bioinorganic-chemistry/Group-V-Arion.html
[b] *Laboratoire National des Champs Magnetiques Intenses-CNRS, 25 Avenue des Martyrs, 38042 Grenoble Cedex 9, France*
[c] *Institute for Oncology and Radiology of Serbia, University of Belgrade, Pasterova 14, 11000 Belgrade, Serbia*
[d] *Institute of Physical Chemistry and Chemical Physics, Slovak University of Technology, Faculty of Chemical and Food Technology, Radlinského 9, 81237 Bratislava, Slovakia*
[e] *Department of Inorganic and Analytical Chemistry, University of Szeged, Dom ter 7, 6720 Szeged, Hungary*
📄 *Supporting information and ORCID(s) from the author(s) for this article are available on the WWW under https://doi.org/10.1002/ejic.201700962.*

★ChemPubSoc
Europe

EurJIC
European Journal
of Inorganic Chemistry

Full Paper

Quite recently, two other members of the TSC family, namely di-2-pyridyl ketone 4-cyclohexyl-4-methyl-3-thiosemicarbazone (DpC) and (E)-N'-(6,7-dihydroquinolin)-8(5H)-ylidene-4-(pyridine-2-yl)piperazine-1-carbothiohydrazide (COTI-2), have entered clinical studies showing multi-target features[19,20] and rekindling the research interest in TSCs.

Besides the good cytotoxicity and the selectivity for cancer cells, very often further anticancer investigations are prohibited because of the low water solubility and high lipophilicity of TSCs. Finding an appropriate hydrophilicity/lipophilicity balance of a potent anticancer drug candidate is still a challenge.[21]

Rapid tumor growth requires increasing amounts of essential metal ions (iron, copper, zinc). Their deficiency makes cancer cells more sensitive to chemotherapeutics compared to normal cells.[11,14,22] Complexes of TSCs with essential transition-metal ions do not always exhibit better in vitro cytotoxicity than metal-free TSCs alone.[2,8,10,15–18] According to the previous studies, only few iron–TSC complexes showed an improved cytotoxic effect upon coordination to iron.[23,24] Although they can activate various pathways leading ultimately to cell apoptosis, their mechanism of inhibition of cell proliferation is still unknown. The formation of reactive oxygen species (ROS) which damage cellular processes and lead to cell apoptosis is a feature often attributed to the anticancer activity of iron(III) complexes of TSCs.[2,25] In addition, L-proline is distinct from other amino acids since it is the only secondary amino acid. The metabolism of proline is different and takes place in the presence of special enzymes. It is accompanied by the formation of signaling ROS for epigenetic reprogramming by oncogenes, and regulates redox homeostasis. These regulatory functions play an important role in apoptosis, autophagy, and hypoxia in the presence of low oxygen levels typical for cancer.[26]

Several years ago, we reported on the synthesis of 3-formyl-2-hydroxy-5-methylbenzyl-L-proline and 3-formyl-2-hydroxy-5-methylbenzyl-D-proline (L-Pro-MSA and D-Pro-MSA, respectively), which are closely related to monophyllidin (Figure 1), a naturally occurring alkaloid with antibacterial effect towards Enterococcus faecalis.[27] By condensation reactions with thiosemicarbazides new thiosemicarbazone–proline hybrids were synthesized, namely L-Pro-STSC and D-Pro-STSC, with improved water solubility and enhanced anticancer activity, particularly, upon the coordination to the metal.[18]
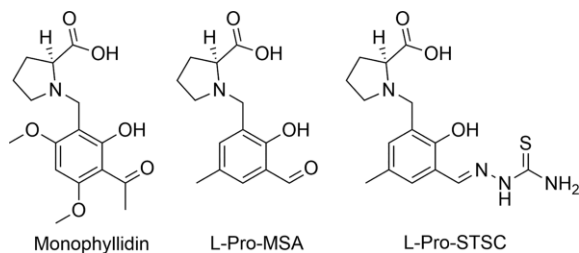

Figure 1. Line drawings of monophyllidin, L-Pro-MSA, and L-Pro-STSC.

These hybrid molecules (L-Pro-STSC and D-Pro-STSC) form mono-ligand complexes with iron(III/II), copper(II), and zinc(II) and, in addition, bis-ligand complexes with iron(III/II).[18] The metal-free hybrids showed only moderate cytotoxic potency to-

wards colon cancer (SW480) and ovarian cancer (CH1) cell lines, while coordination to copper(II) markedly increased their cytotoxicity. The replacement of the phenolic moiety (in L-Pro-STSC) by pyridine [in 3-methyl-(S)-pyrrolidine-2-carboxylate-2-formyl-pyridine thiosemicarbazone, L-Pro-FTSC] did not significantly improve the cytotoxic properties of the hybrids, most probably because of further enhancement of the hydrophilic character.[21] The structural modifications at the terminal N atom of the TSC moiety in L-Pro-STSC and coordination to essential metals had a beneficial impact on the cytotoxicity, while the changes on the proline moiety of the hybrids reduced antiproliferative activity.[28] The results prompted us to extend the series of L-Pro-STSC conjugates by attachment of aromatic groups at the terminal N atom of TSCs to increase their lipophilic character, and hopefully their cytotoxic potency. We anticipated that L-Pro-STSC (H_2L^1), Pyrr-L-Pro-STSC (H_2L^2), and two other conjugates, namely phenyl-L-Pro-STSC (H_2L^3) and 2-naphthyl-L-Pro-STSC (H_2L^4), will form mono-ligand complexes with iron(III) providing better insight into (i) the role of iron coordination and its effect on antiproliferative activity, (ii) the effect of aromatic groups at the terminal N atom on the antiproliferative activity of the conjugates as well as that of their iron(III) complexes.
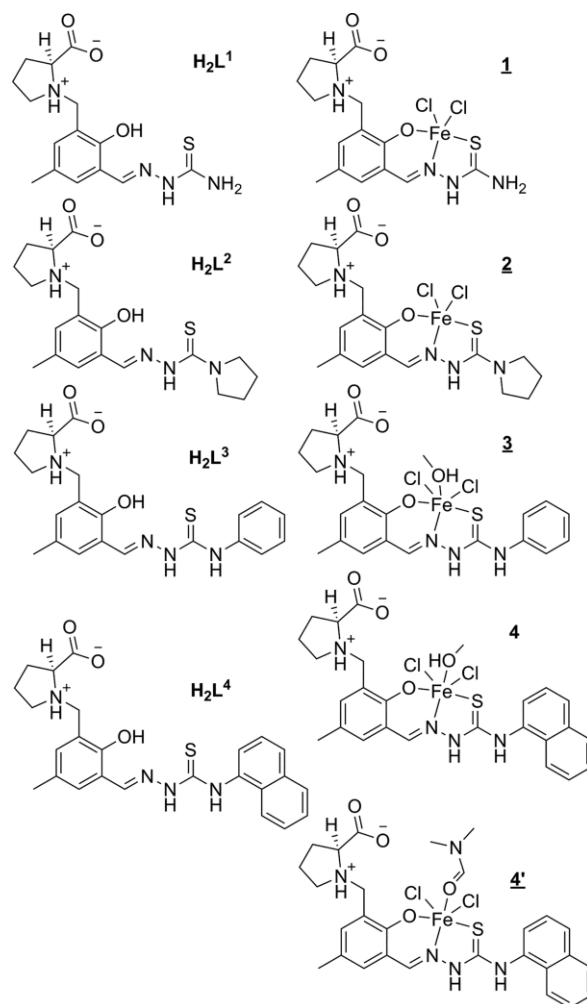

Figure 2. Line drawings of the L-Pro-STSC hybrids and their iron(III) complexes studied in this work. Underlined numbers indicate complexes studied by X-ray diffraction. Co-crystallized solvent molecules were omitted.

ChemPubSoc
Europe

EurJIC
European Journal
of Inorganic Chemistry

Full Paper

Herein we report on the synthesis and characterization of two N-monosubstituted L-Pro-STSC conjugates (**H₂L³** and **H₂L⁴**) and five iron(III) complexes (**1–4** and **4′**) which have been prepared and isolated in the solid state (Figure 2) and characterized by elemental analysis, spectroscopic methods, magnetic susceptibility measurements, electrochemistry, and X-ray diffraction.

In particular, coordination chemistry of the hybrids [L-Pro-STSC (**H₂L¹**), pyrrolidyl-L-Pro-STSC (**H₂L²**), phenyl-L-Pro-STSC (**H₂L³**), and 2-naphthyl-L-Pro-STSC (**H₂L⁴**)], the effects of iron(III) coordination and N-terminal substitution of the TSC moiety on cytotoxicity in five human and one murine cancer cell lines, namely cervical cancer cells (HeLa), melanoma cells (FemX), adenocarcinoma alveolar basal cells (A549), colon cancer cells (LS-174), breast cancer cells (MDA-MB-453), murine transformed endothelial cell line (MS1), and noncancerous fetal lung fibroblast (MRC-5) have been investigated and discussed.

Results and Discussion

Synthesis and Characterization of the Ligand Precursors

The chiral proligands L-Pro-STSC (**H₂L¹**) and Pyrr-L-Pro-STSC (**H₂L²**) have been synthesized as described previously.[18,28] The reaction of L-Pro-MSA with 4-phenyl-3-thiosemicarbazide in ethanol/water mixture and 4-(1-naphthyl)-3-thiosemicarbazide in ethanol afforded **H₂L³** and **H₂L⁴** in 64 and 65 % yield, respectively. ESI mass spectra of **H₂L³** and **H₂L⁴** measured in negative ion mode showed characteristic peaks with m/z 411 and 461 attributed to $[M - H]^-$, while those measured in positive ion mode revealed peaks with m/z 413 and 485, respectively, assigned to $[M + H]^+$ and $[M + Na]^+$. The formation of proline–thiosemicarbazone hybrids **H₂L³** and **H₂L⁴** was also confirmed by one-dimensional (¹H and ¹³C) and two-dimensional (¹H–¹H COSY, ¹H–¹³C HMBC, and HSQC) NMR measurements (see Experimental Section and Figures S1–S14).

Synthesis and Characterization of Iron(III) Complexes

Iron(III) complexes **1–3** have been prepared by reaction of FeCl₃·6H₂O with the corresponding proligand (**H₂L¹**, **H₂L²**, or **H₂L³**) in methanol. A small excess of iron(III) salt (ca. 0.3 equiv.) assured the formation of the mono-ligand complexes [Fe(**HL¹⁻³**)Cl₂]. Vapor diffusion of Et₂O in methanolic solution of the complexes afforded X-ray diffraction quality crystals of **1–3** in 25, 33, and 61 % yield, respectively. Complex **4** resulted from the reaction of FeCl₃·6H₂O with **H₂L⁴** in ethanol/water mixture (1:1). Evaporation of the solvent under reduced pressure followed by dissolution of the residue in methanol and precipitation with Et₂O gave rise to pure solid **4**. By vapor diffusion of Et₂O into the solution of **4** in dimethylformamide (DMF) single crystals of **4′** were obtained.

All iron(III) complexes were characterized by elemental analysis, IR (Figures S15–S19), UV/Vis, CD spectroscopy, and ESI mass spectrometry. ESI mass spectra of iron(III) complexes in negative ion mode exhibit strong peaks with m/z 459, 514, 537, and 586, respectively, attributed to $[Fe(\mathbf{L^1})Cl_2]^-$, $[Fe(\mathbf{L^2})Cl_2]^-$, $[Fe(\mathbf{L^3})Cl_2]^-$, and $[Fe(\mathbf{L^4})Cl_2]^-$, while in positive ion mode peaks assigned to $[Fe(\mathbf{L^{1-4}})]^+$ were observed (see Experimental Section). UV/Vis spectra of **1–4** in methanol and **4′** in DMF showed intraligand transitions and metal-to-ligand charge-transfer bands between 250 and 600 nm (Figures S20–S24). In CD spectra of **1–4** (Figure S25) the presence of enantiomeric excess was observed because of the chiral L-proline moiety in the complexes. The structures of the iron complexes in the solid state were established by single-crystal X-ray diffraction.

X-ray Crystallography

The results of X-ray diffraction studies of **1**, **2**·0.2CH₃OH· 0.125Et₂O·0.063H₂O, **3**·0.5CH₃OH, and **4′**·Et₂O are shown in Figure 3 and Figure 4, respectively, with selected geometric param-
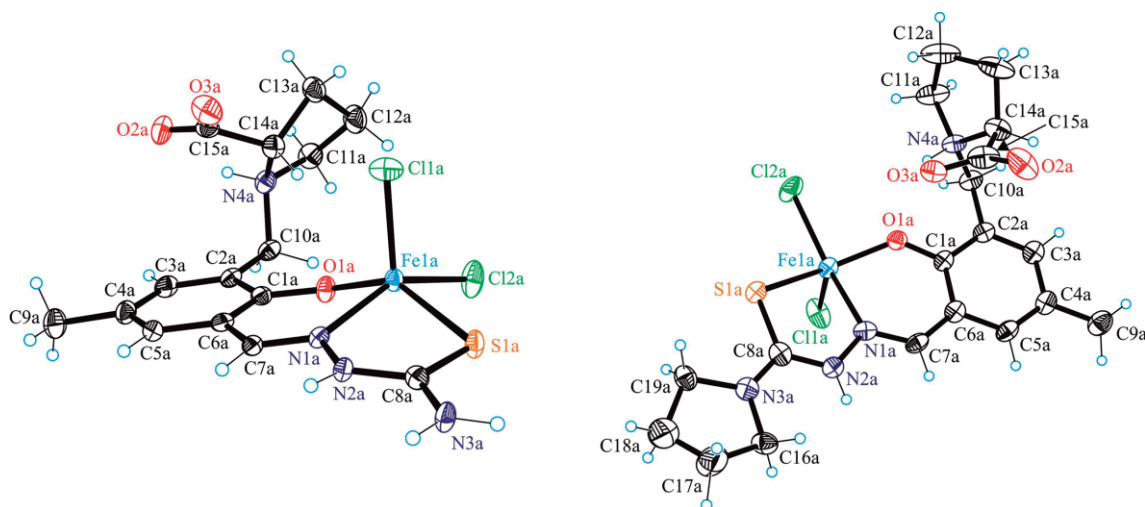

Figure 3. ORTEP views of **1** (left) and **2** (right) with atom labeling scheme. Thermal ellipsoids were drawn at the 50 % probability level. Selected bond lengths [Å] and bond angles [°] in **1**: Fe1a–O1a 1.878(2), Fe1a–N1a 2.193(2), Fe1a–S1a 2.3585(9), Fe1a–Cl1a 2.2245(8), Fe1a–Cl2a 2.2616(8), C1a–O1a 1.315(4), N1a–N2a 1.387(3), N2a–C8a 1.327(4), C8a–S1a 1.707(3), C8a–N3a 1.322(4); O1a–Fe1a–N1a 82.81(9), N1a–Fe1a–S1a 78.52(7); in **2**: Fe1a–O1a 1.899(4), Fe1a–N1a 2.148(5), Fe1a–S1a 2.3769(17), Fe1a–Cl1a 2.2332(18), Fe1a–Cl2a 2.2473(19), C1a–O1a 1.311(7), N1a–N2a 1.383(7), N2a–C8a 1.335(8), C8a–S1a 1.726(7), C8a–N3a 1.307(8); O1a–Fe1a–N1a 84.00(19), N1a–Fe1a–S1a 78.70(15). The solvent molecules were omitted for clarity.

ChemPubSoc
Europe

EurJIC
European Journal
of Inorganic Chemistry

Full Paper

eters quoted in the legends. Compounds **1**–**3** and **4′** crystallized in the noncentrosymmetric space groups $P1$, $P3_12_1$, $P2_1$, and $P2_12_12_1$, respectively, as pure enantiomers, as confirmed by the Flack parameters in Table 1. The asymmetric unit of **1** consists of four independent molecules of the iron(III) complex [Fe(**HL¹**)Cl₂], while that of **2**·0.2CH₃OH·0.125Et₂O·0.063H₂O is composed of two crystallographically independent molecules of [Fe(**HL²**)Cl₂] and co-crystallized solvent.

The ligands in complexes **1** and **2** act as tridentate mono-protonated species (**HL¹**)⁻ and (**HL²**)⁻ coordinating to iron(III) through the phenolato oxygen atom O1a, the nitrogen atom N1a, and the thione sulfur S1a as shown for one crystallographically independent complex in Figure 3. The coordination polyhedron of iron(III) is close to square-pyramidal (τ is 0.12 and 0.15 in **1** and **2**, respectively)[29] and is completed by two chlorido ligands, one in the basal plane, while another in the
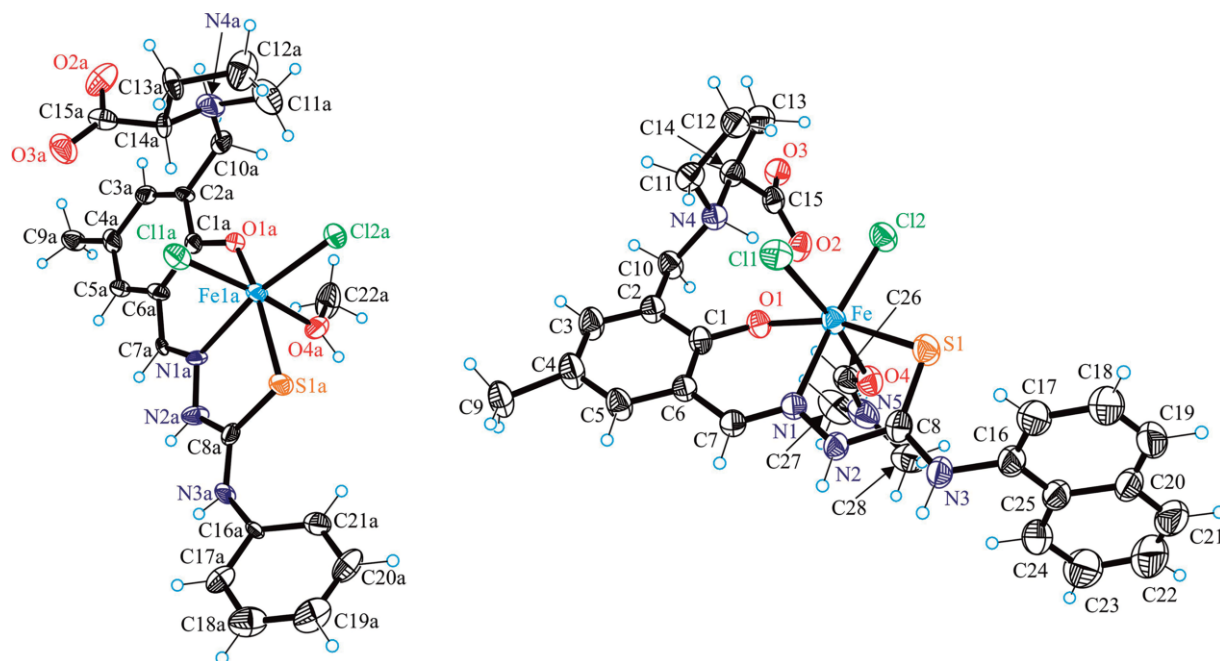

Figure 4. ORTEP view of **3** (left) and **4′** (right) with atom labeling scheme. Thermal ellipsoids were drawn at the 50 and 30 % probability level, respectively. Selected bond lengths [Å] and bond angles [°] in **3**: Fe1a–O1a 1.896(2), Fe1a–N1a 2.188(6), Fe1a–S1a 2.431(2), Fe1a–Cl1a 2.333(2), Fe1a–Cl2a 2.303(2), Fe1a–O4a 2.182(6), C1a–O1a 1.307(9), N1a–N2a 1.379(8), N2a–C8a 1.338(9), C8a–S1a 1.709(8), C8a–N3a 1.333(9); O1a–Fe1a–N1a 86.7(2), N1a–Fe1a–S1a 78.85(16); in **4′**: Fe–O1 1.923(2), Fe–N1 2.178(3), Fe–S1 2.4167(10), Fe–Cl1 2.3633(11), Fe1–Cl2 2.2915(11), Fe–O4 2.101(4), C1–O1 1.320(4), N1–N2 1.380(4), N2–C8 1.347(5), C8–S1 1.701(4), C8–N3 1.328(5); O1–Fe–N1 84.36(10), N1–Fe–S1 80.02(8). The solvent molecules were omitted for clarity.

Table 1. Crystal data and details of data collection for iron(III) complexes.

Compound	**1**	**2**·0.2CH₃OH·0.125Et₂O·0.063H₂O	**3**·0.5CH₃OH	**4′**·Et₂O
Formula	$C_{15}H_{19}Cl_2FeN_4O_3S$	$C_{19.7}H_{27.18}Cl_2FeN_4O_{3.39}S$	$C_{22.5}H_{29}Cl_2FeN_4O_{4.5}S$	$C_{32}H_{42}Cl_2FeN_5O_5S$
F_w [g mol⁻¹]	462.15	533.04	586.30	735.51
Space group	$P1$	$P3_12_1$	$P2_1$	$P2_12_12_1$
a [Å]	11.7228(4)	15.2992(7)	10.0939(3)	15.2295(3)
b [Å]	13.1340(5)	15.2992(7)	19.8953(6)	13.2442(3)
c [Å]	14.2125(8)	39.998(2)	12.8165(4)	17.1575(3)
α [°]	106.120(2)			
β [°]	97.415(2)		101.140(2)	
γ [°]	113.163(2)			
V [Å³]	1861.10(14)	8107.9(7)	2525.33(13)	3460.71(12)
Z	4	12	4	4
λ [Å]	0.71073	0.71073	0.71073	1.54186
$\varrho_{calcd.}$ [g cm⁻³]	1.649	1.310	1.704	1.412
Crystal size [mm]	0.20 × 0.16 × 0.16	0.40 × 0.23 × 0.15	0.08 × 0.01 × 0.01	0.22 × 0.05 × 0.04
T [K]	120(2)	100(2)	100(2)	100(2)
μ [mm⁻¹]	1.233	0.860	7.849	5.865
R_1[a]	0.0235	0.0609	0.0614	0.0485
wR_2[b]	0.0629	0.1731	0.1549	0.1364
Flack parameter	–0.002(8)	0.04(3)	–0.001(7)	–0.011(5)
GOF[c]	1.020	1.177	1.003	1.000

[a] $R_1 = \Sigma||F_o| - |F_c||/\Sigma|F_o|$. [b] $wR_2 = \{\Sigma[w(F_o^2 - F_c^2)^2]/\Sigma[w(F_o^2)^2]\}^{1/2}$. [c] GOF $= \{\Sigma[w(F_o^2 - F_c^2)^2]/(n - p)\}^{1/2}$, where n is the number of reflections and p is the total number of parameters refined.

apical position. The proline moiety adopts the zwitterionic form and is not involved in the coordination to iron(III).

Protonation of N4a makes this atom chiral in addition to C14a. Both atoms adopt the same S configuration as observed recently in complexes of nickel(II), palladium(II), and copper(II) with the same type of proline–thiosemicarbazone hybrids.[18,28] Opposite configurations of these two atoms are also well documented in the literature.[21,30]

The iron(III) atom comes out from the basal plane defined by donor atoms O1a, N1a, S1a, and Cl2a towards Cl1a in **1** and **2** by 0.579 and 0.561 Å, respectively. In complexes **3** and **4′** the ligands (**HL³**)⁻ and (**HL⁴**)⁻ are bound to iron(III) similarly. However, iron(III) in **3** and **4′** adopts a distorted octahedral coordination geometry with one chlorido ligand and one molecule of solvent (methanol or DMF) in axial positions, and another chlorido ligand, along with three donor atoms of the corresponding tridentate ligand occupying the equatorial coordination places as shown in Figure 4. The increase of coordination number in **3** and **4′** is presumably due to the presence of electron-withdrawing substituents at the terminal thioamide nitrogen atom of the thiosemicarbazide moiety in both these complexes, which decreases the electron density at the iron atom. As a result the affinity for a sixth ligand (methanol or DMF) increases.

The Fe–O, Fe–N, Fe–S, and Fe–Cl bond lengths in **3** and **4′** are markedly longer than those in a series of iron(III) complexes with 2-hydroxy-1-naphthaldehyde-thiosemicarbazones reported recently.[24] This is probably due to the different coordination numbers in the two types of compounds and reduced ligand–ligand repulsions in five-coordinate iron(III) complexes with 2-hydroxy-1-naphthaldehyde-thiosemicarbazones.[24]

The carboxylate group of the proline moiety is not coordinated to iron(III). Instead it is involved in formation of noncentrosymmetric dimeric associates through hydrogen bonds with nitrogen atoms of the thiosemicarbazide fragment as shown in Figures S26–S29. Five-coordinate and six-coordinate complexes **1** and **3** form dimeric associates through the same set of hydrogen bonds. Even though the formation of dimeric associates is also found in the crystal structure of **2** (Figure S27), a dissimilar type of hydrogen bonding involved is due to the absence of a terminal nitrogen as a proton donor as was the case for **1** and **3**. In **4′** the presence of a bulky naphthyl group at the terminal nitrogen proton donor precludes the formation of dimeric associates. Instead the molecules of **4′** are building a 1D chain of H-bonded molecules with a two-molecule portion shown in Figure S29.

Solution Speciation and UV/Vis Measurements for Monitoring the Stability of Iron(III) Complexes

The solution stability of complexes **1–4** was investigated following the changes of UV/Vis bands in the region of 200–700 nm in MeOH and in MeOH/H₂O (1:1) solutions. UV/Vis spectra of methanolic solutions of **1–4** did not show marked changes of the solutions even after seven days of standing at room temperature (Figures S20–S24). Compounds **1** and **2** were stable in MeOH/H₂O (1:1) over 15 h, while complex **3** underwent

changes after 30 min in MeOH/H₂O (1:1) solution at room temperature. The formation of precipitate was observed after 15 h (Figures S30–S32). These changes are partly due to the limited solubility of complex **3** under the given conditions, although the spectral changes indicate some decomposition of the complex as well. The solution speciation of the iron(III)–**H₂L¹** system was determined in a 30 % (w/w) DMSO/H₂O mixture in our recent work[18] by using pH-potentiometric and UV/Vis spectrophotometric titrations. Results revealed the formation of monoligand complexes such as [Fe(**HL¹**)]²⁺, [Fe(**L¹**)]⁺, and bis-ligand complexes [Fe(**HL¹**)(**L¹**)], [Fe(**L¹**)₂]⁻, and [Fe(**L¹**)₂(OH)]²⁻ (depending on the conditions, e.g., metal-to-ligand ratio, pH). The protonated iron(III) complexes containing (**HL¹**)⁻ are formed typically in the acidic pH range, and the stability of the bis-ligand complex [Fe(**L¹**)₂]⁻ is very high. As a consequence complex **1** with the original [Fe(**HL¹**)]²⁺ composition most probably has a different stoichiometry after dissolution in the aqueous solution. The pK_a of this complex is 2.91.[18] This indicates the complete deprotonation of the noncoordinating hydrazinic N²–H atom at pH > 4.5. This deprotonation is accompanied by significant spectral changes as shown in Figure S33. However, the spectra remain practically unchanged at pH values between about 6 and 10 as a result of the formation of the [Fe(**L¹**)₂]⁻ complex even at 1:1 metal-to-ligand ratio. (Notably, these spectra are fairly similar to those recorded at 1:2 metal-to-ligand ratio at a pH between 6.8 and 9.8.[18]) On the basis of the reported stability constants, concentration–distribution curves were calculated for complex **1** (Figure 5), which suggest that the proligand is mostly bound in the bis-ligand complex [Fe(**L¹**)₂]²⁺ at pH 7.4 in solution. It should be also noted that the stability of the iron(III) complexes is significantly higher than that of the iron(II) species.[18]
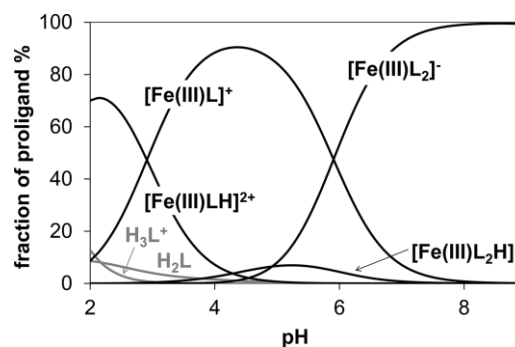

Figure 5. Concentration–distribution curves for complex **1** in the pH range from 2 to 8 calculated on the basis of stability constants taken from ref.[18] [$c_{complex\ 1}$ = 1.0 × 10⁻³ M; T = 298 K, I = 0.10 M (KCl) in 30 % (w/w) DMSO/H₂O].

Similar complexation processes and stoichiometry of the complexes are assumed for the other three proligands **H₂L²**–**H₂L⁴** as they coordinate in a similar manner, namely through the O, N, S⁻ donor set, but most likely the stability of the complexes somewhat differs because of the presence of different substituents at the terminal nitrogen atom of the thiosemicarbazide moiety. The substituents at the N-terminal position are located quite close to the sulfur atom which is involved in the coordination. The electron-donating methyl substituents

ChemPubSoc
Europe

EurJIC
European Journal
of Inorganic Chemistry

Full Paper

have an unambiguous effect on the electron distribution in the thioamide moiety and thus on the coordination bond as well. In the case of the α-N-pyridyl thiosemicarbazones the increased stability of the iron(III/II) complexes by the N-terminal dimethylation is well documented in one of our previous papers.[31] Based on the solution speciation data, the iron(III) complexes of salicylaldehyde (and α-N-pyridyl thiosemicarbazones) show a more favored formation of bis complexes over the mono species. As a consequence, at 1:1 metal-to-ligand ratio not only are mono species formed, but also bis complexes. It results in the appearance of unbound iron(III) ions which tend to hydrolyze without the presence of other chelating agents. In the biological assays no precipitation occurred (or it was not visible) as the free iron(III) was most probably complexed by the components of the applied medium.

Magnetic Susceptibility Measurements

The temperature dependence of the magnetic susceptibility ($\chi_M T$) for complexes **2** and **4** was measured and a Curie plot is shown in Figure S34. At room temperature, the $\chi_M T$ product is equal to 4.25 mL K mol^{-1} for **2** and 4.30 mL K mol^{-1} for **4**. These values correspond well to the isolated high-spin iron(III) (S = 5/2)[32] with isotropic g values 1.97 and 1.98 for **2** and **4**, respectively. At low temperature a sharp decrease of $\chi_M T$ values is observed. Taking into account the mononuclear structure of **2** and **4** this behavior is, presumably, due to the non-negligible zero field splitting (ZFS)[33] of iron(III), as well as to the presence of intermolecular interactions in **2** and **4**.

Electrochemistry

The electrochemical experiments on selected iron complexes were performed in MeCN/nBu$_4$NPF$_6$ solution with a platinum working electrode at a scan rate of 100 mV s^{-1}. As shown in Figure 6 the cathodic peak potential E_{pc} of the iron(III)/iron(II) redox couple is −0.87 V, −0.80 V, and −0.78 V versus Fc$^+$/Fc (−0.23 V, −0.16 V, and −0.14 V vs. NHE) for **1**–**3**, respectively. Complex **4** exhibits similar redox behavior compared to **3** with the less negative cathodic peak potential at −0.73 V versus

Fc$^+$/Fc (see violet trace in Figure 6). However, we observed an additional reduction peak at even less negative peak potential at −0.54 V indicating more complex redox behavior.
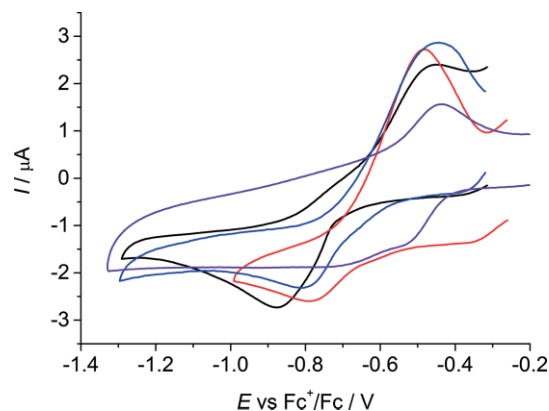

Figure 6. The cyclic voltammograms of 0.5 mM of **1** (black trace), **2** (blue trace), **3** (red trace), and **4** (violet trace) in MeCN/nBu$_4$NPF$_6$ at a scan rate of 100 mV s^{-1}.

The corresponding cyclic voltammograms showed one reduction peak with a strongly shifted reoxidation peak (peak-to-peak separation around 400 mV) exhibiting typical features of a slow electron process. The shape of the cyclic voltammograms in the reverse scan additionally indicates a weakly adsorbed reduction product, where a desorption characteristic for redissolution of presumably less soluble iron(II) species upon reoxidation to the iron(III) state occurs. Therefore, for simulation of the corresponding cyclic voltammograms a small rate constant for the heterogeneous electron transfer was used (k_s = 2.5×10^{-4} cm s^{-1} for **1**, k_s = 1×10^{-3} cm s^{-1} for **2**, and k_s = 5×10^{-4} cm s^{-1} for **3**). As shown in Figure S35 a fairly good fit was achieved taking into account additionally the adsorption of the reduced species on the electrode surface (Γ_{max} = 5×10^{-6}, 1×10^{-5}, and 8×10^{-6} for **1**$^-$, **2**$^-$, and **3**$^-$, respectively) providing further evidence for adsorption processes. The simulation enabled us to determine the formal redox potentials for the investigated iron complexes ($E^{o\prime}$ = −0.67 V for **1**, −0.65 V for **2**, and −0.65 V for **3**, all vs. Fc$^+$/Fc). These low redox potentials clearly occur within the biologically accessible window (−0.4 to

Table 2. IC$_{50}$ values after inhibition of cell growth by the hybrids **H$_2$L^1**–**H$_2$L^4** and complexes **1**–**4** in six cancer cell lines (A549, FemX, HeLa, LS-174, MDA-MB-453, and MS1) and noncancerous cell line (MRC-5).

IC$_{50}$ [μM] (value, SD)[a]							
	A549	FemX	HeLa	LS-174	MDA-MB-453	MS1	MRC-5
H$_2$L^1	> 300[b]	> 300[b]	> 300[b]	> 300[b]	> 300[b]	> 300[b]	> 300[b]
H$_2$L^2	271 ± 11	221 ± 12	240 ± 5	295 ± 0	> 300[b]	207 ± 4	203 ± 2
H$_2$L^3	141 ± 4	31 ± 2	146 ± 7	48 ± 3	> 300[b]	125 ± 8	211 ± 9
H$_2$L^4	212 ± 1	15 ± 2	120 ± 7	135 ± 3	109 ± 1	20 ± 3	204 ± 10
1	51 ± 7	53 ± 3	61 ± 3	91 ± 6	39 ± 1	44 ± 3	26 ± 2
2	53 ± 3	25 ± 5	57 ± 2	60 ± 7	28 ± 1	33 ± 1	41 ± 2
3	72 ± 1	54 ± 2	52 ± 4	87 ± 3	40 ± 1	39 ± 3	52 ± 3
4	78 ± 9	24 ± 1	78 ± 8	89 ± 5	66 ± 0	25 ± 0	24 ± 1
Cisplatin[c]	17 ± 1[c]	11 ± 1	8 ± 2[c]	22 ± 7	21 ± 6	n.d.	30 ± 3[c]

[a] IC$_{50}$ values were calculated as mean values obtained from three independent experiments after 48 h of cell exposure in the MTT assay. IC$_{50}$ values are quoted with their standard deviations (SD). [b] The sign > indicates that the IC$_{50}$ value is not reached in the examined range of concentrations. [c] IC$_{50}$ values for cisplatin were taken from ref.[37] The tested compounds were applied at the following concentrations: 18.75; 37.5; 75; 150; 300 μM.

★ ChemPubSoc
   Europe

EurJIC
European Journal
of Inorganic Chemistry

Full Paper

+0.8 V vs. NHE) using the known $E_{1/2}$ of ferrocene (+0.64 V) versus standard hydrogen electrode (SHE).[34] These results are comparable with those reported for other iron(III)–TSC complexes.[35,36] Such redox active complexes are able to markedly increase the amount of ROS in cancer cells. Hydroxyl radicals in such systems can be obtained from Fenton reactions, where the iron cycles between the Fe^{II} and Fe^{III} oxidation states.

Cytotoxicity

The cytotoxic potential of hybrids H_2L^1–H_2L^4 and the four iron(III) complexes **1**–**4** was investigated in five human cancer cell lines and one murine cancer cell line, namely HeLa, FemX, A549, LS-174, MDA-MB-453, and MS1, as well as in one noncancerous cell line MRC-5 by means of the colorimetric MTT assay. The derivatives H_2L^1–H_2L^4 and their iron(III) complexes **1**–**4** show IC_{50} values in the range from 14.7 to > 300 µM (Table 2). None of the compounds tested has reached the level of cytotoxicity of cisplatin on investigated cancer cell lines. The following structure–activity relationships were established: (i) the impact of substitution at terminal NH_2 group of TSC moiety, (ii) impact of metal coordination of the hybrids, and (iii) metal identity.

Substitution at the Terminal N Atom of the TSC Moiety

The favorable effect of terminal N-atom substitution of the hybrid H_2L^1 by a pyrrolidinyl group in H_2L^2, a phenyl group in H_2L^3, and a naphthyl group in H_2L^4 was observed by an increase of the cytotoxic potency in the following order: H_2L^1 < H_2L^2 < H_2L^3 < H_2L^4 in all cancer cell lines except LS-174. In the latter, the rank order was H_2L^1 < H_2L^2 < H_2L^4 < H_2L^3. H_2L^2 showed a slightly better activity compared to H_2L^1 in all cancer cell lines. The substitution with aromatic groups (hybrids H_2L^3 and H_2L^4) resulted in a two- to more than 20-fold increase of cytotoxic potency of the hybrids in all cancer cell lines. Cancer cell lines FemX and MS1 were most sensitive to substitution of one H atom at the terminal NH_2 group of the TSC moiety by a naphthyl group (hybrid H_2L^4). IC_{50} values of 15 µM in FemX and 20 µM in MS1 cell lines indicate an about 20- and 15-fold increase of cytotoxicity compared to H_2L^1.

In the cell line MDA-MB-453 the positive effects of ligand substitution and metal coordination are also obvious. Introduction of the naphthyl group increased the cytotoxicity, while coordination to iron enhanced it by a factor of two. According to the IC_{50} values, introduction of the naphthyl group increased the cytotoxicity of H_2L^1 by about three times, whereas coordination to iron improved the cytotoxicity of H_2L^1 by about eight times (complex **1**).

Notably, H_2L^1 is mainly present in H_2L (75 %) and HL^- (25 %) forms in aqueous solution at pH 7.4 based on its pK_a values.[18] H_2L has a zwitterionic structure containing negatively charged carboxylate and protonated proline nitrogen moieties, and HL^- is formed by the deprotonation of the phenolic OH group. In all, these features strongly contribute to the relatively high hydrophilicity of compound H_2L^1 (log $D_{7.4}$ = –0.56).[18] Its derivatives H_2L^3 and H_2L^4 are most probably more lipophilic due to the presence of the phenyl and naphthyl groups, what is advantageous for the easier passage through the biological membranes resulting in the increased cytotoxicity. The drug delivery and activity of the iron complexes might be improved by attaching them to a prodrug carrier as recently published for a series of related iron complexes.[24] All those iron complexes possess one tridentate Schiff base ligand (modified just at the terminal N atom), one iron center, and two chloride ligands (as leaving groups).[24]

Metal Coordination

Iron(III) complexes **1** and **2** showed an improved antiproliferative activity compared to their corresponding metal-free ligands in all cancer cell lines, which may be a consequence of the altered size, lipophilicity, and charge upon complex formation. The strongest effect of iron coordination on cytotoxicity (ca. nine-fold increase) compared to the corresponding metal-free ligand, was observed for **2** in FemX cell line. On the other hand, coordination of the hybrids with aromatic substituents (H_2L^3 and H_2L^4) to iron in **3** and **4** showed mixed results with an increase of cytotoxic activity in HeLa, A549, and MDA-MB-453 cell lines and reduction of cytotoxic activity in MS1, LS-174, and FemX. According to the IC_{50} values, an improved cytotoxic activity of iron(III) complexes towards the investigated cell lines could be attributed to their contribution to ROS generation, as previously reported,[23,35] in addition to the increase of their lipophilicity by introduction of bulky aromatic groups.

Metal Identity

The coordination of H_2L^2 to iron(III) increases the antiproliferative activity by a factor of five in A549 cell lines what is comparable with recently reported results for the same hybrid and its nickel(II), palladium(II), and copper(II) mono-ligand complexes.[28] The coordination to nickel(II) and palladium(II) led to a drop of cytotoxic potency of H_2L^2, while coordination to copper increased it by a factor of 9.5. Taking together, the following order of cytotoxic activity could be presented for nickel(II), palladium(II), copper(II), and iron(III) complexes of H_2L^2 of 1:1 stoichiometry in A549 cancer cell lines: Ni^{II} < Pd^{II} < H_2L^2 < Fe^{III} (five fold) < Cu^{II} (9.5 fold).

Selectivity

By comparing the IC_{50} values measured in the tested cancerous and the noncancerous cell lines it can be concluded that all compounds showed poor selectivity or no selectivity to cancer cell lines. The proligands H_2L^3 and H_2L^4 possess slightly better selectivity to cancer cells compared to their corresponding iron(III) complexes, where the selectivity is absent.

Conclusions

Two hybrids H_2L^3 and H_2L^4, and five iron(III) complexes **1**–**4** and **4′** were synthesized, characterized by spectroscopic, ESI-

★ ChemPubSoc
Europe

EurJIC
European Journal
of Inorganic Chemistry

Full Paper

MS, electrochemical, and magnetic susceptibility methods, and their antiproliferative activity against six human and murine cancer cell lines and one normal cell line was studied. The substitution at the terminal NH_2 group of the TSC moiety of the hybrids induces a positive cytotoxic effect, which may be attributed to their hydrophilicity/lipophilicity balance.

Iron(III) complexes were isolated in the solid state and their structure was confirmed by X-ray diffraction measurements, mass spectrometry, and elemental analysis. Attachment of aromatic groups to the terminal N atom of the TSC moiety favors octahedral coordination geometry of the central iron atom, while introduction of aliphatic groups induces square-pyramidal coordination geometry, which is attributed to the electron-withdrawing or electron-donating effect of the substituents at the terminal N atom of the TSC moiety of the hybrids. Thus, the hybrids H_2L^1 and H_2L^2 with iron(III) form square-pyramidal complexes [Fe(HL^1)Cl_2] (**1**) and [Fe(HL^2)Cl_2]·1.6H_2O (**2**), while H_2L^3 and H_2L^4 form octahedral complexes [Fe(HL^3)(MeOH)Cl_2]· 0.5H_2O (**3**) and [Fe(HL^4)(DMF)Cl_2]·0.5Et_2O·H_2O (**4′**). However, these differences observed in the solid state are not characteristic for their behavior in solution. Instead, favored formation of bis-ligand iron(III) complexes is observed, in addition to mono-ligand complexes, at physiological pH.

The substitution at the terminal NH_2 group of the TSC moiety of H_2L^1 by pyrrolydinyl, phenyl, and naphthyl groups enhances the antiproliferative activity of all hybrids in all investigated cancer cell lines with exception of colon cancer cell line LS-174 where the cytotoxicity follows the order $H_2L^1 < H_2L^2 < H_2L^4 < H_2L^3$. Iron(III) complexes **1**–**4** showed better cytotoxic potency compared to their corresponding hybrids with exception of complex **3** in LS-174 cell line, complex **4** in MS1 cell line, and complexes **3** and **4** in FemX, where they showed reduced cytotoxicity compared to their parent hybrids. On the other hand, neither hybrids nor complexes displayed significant selectivity toward cancerous cells over normal cells. In general, structural modification at the terminal N atom of the TSC moiety of the hybrids, especially by introducing aromatic groups, has significant impact on cytotoxicity. Metal coordination causes beneficial effects on cytotoxic activity, particularly in the case of essential transition metals (iron and copper). The metal identity affects the cytotoxic potency of the hybrids in agreement to our previous work in such a manner that essential metals (iron and copper) improve the cytotoxicity of the metal-free ligands, while other transition metals (Ni and Pd) reduce it.

Experimental Section

Chemicals: All reagents were used as purchased from commercial suppliers. 4-Phenyl-3-thiosemicarbazide and 1-isothiocyanato-naphthalene were purchased from Sigma Aldrich, L-proline from Alfa Aesar, and $FeCl_3$·6H_2O from Riedel-de-Haën. 4-(1-Naphthyl)-3-thiosemicarbazide was synthesized as described in the literature with 30 % yield.[38]

Synthesis of Proligands: The synthesis of H_2L^1·1.5H_2O was previously reported.[18] 2-Hydoxy-3-methyl-(S)-pyrrolidine-2-carboxylate-5-methylbenzaldehyde (L-Pro-MSA) was prepared in 34 % yield, starting from L-proline instead of methyl L-proline ester hydrochloride. The reaction product was purified by column chromatography

by using MeOH/CHCl₃ (1:25) as the eluent. H_2L^2·2H_2O was synthesized by following a previously published procedure.[28]

H_2L^3·2H_2O: To a solution of L-Pro-MSA (740 mg, 2.82 mmol) in ethanol (5 mL) whilst stirring was added a solution of 4-phenyl-3-thiosemicarbazide (470 mg, 2.82 mmol) in water (5 mL). The reaction mixture was heated to reflux at 85 °C for 30 min and then cooled to room temperature and allowed to stand at 5 °C overnight. The precipitate was filtered off, washed with cold EtOH/H_2O (1:1), and dried in vacuo. Yield: 64.0 % (0.70 g). $C_{21}H_{24}N_4O_3S$·2H_2O (448.54): calcd. C 56.29, H 6.30, N 12.49, S 7.15; found C 56.45, H 5.87, N 12.62, S 7.18. ¹H NMR [500 MHz, $(CD_3)_2SO$, 25 °C]: δ = 11.82 (s, 1 H, C=N-NH), 11.62 (s, 1 H, C_{Ph}-OH), 10.03 (s, 1 H, HN-C_{Ph}), 8.51 (s, 1 H, HC=N), 7.88 (s, 1 H, C^6H), 7.58 (d, J = 7.7 Hz, 2 H, $C^{14}H$), 7.38 (t, J = 7.7 Hz, 2 H, $C^{15}H$), 7.22 (t, J = 7.7 Hz, 2 H, $C^{16}H$) 6.98 (s, 1 H, C^4H), 4.16 (d, J = 13.33 Hz, 1 H, CH_2), 3.52 (d, J = 13.33 Hz, 1 H, CH_2 peak partial overlapped with DHO proton signal), 2.91 (br. s, 1 H, proline), 2.43 (br. s, 1 H, proline), 2.29–2.19 (m, 1 H, proline), 2.23 (s, 3 H, CH_3), 1.93–1.80 (m, 2 H, proline), 1.77–1.67 (m, 1 H, proline) ppm. ¹³C{¹H} NMR [126 MHz, $(CD_3)_2SO$, 25 °C]: δ = 178.23 (C=S), 174.96 (CO_2^-), 154.82 (C_{Ph}-OH), 140.23 (HC=N), 136.66 (C^{13}) 134.18 (C^{Ar}), 132.14 (C^4), 128.52 (C^{15}), 127.79 (C^5), 126.47 (C^{14+6}), 126.49 (C^6), 123.51 (C^3), 120.41 (C^1), 65.63 (CH, proline), 56.41 [CH₂(8)], 53.08 (CH₂, proline), 29.46 (CH₂, proline), 23.47 (CH₂, proline), 20.55 (C^7H_3) ppm. ESI-MS (MeOH, positive): m/z = 413 [H_2L^3 + H]⁺. ESI-MS (MeOH, negative): m/z = 411 [HL^3]⁻. UV/Vis (MeOH): λ (ε, M^{-1} cm⁻¹) = 219 (19 891) 340 (19859) 310 (18500) nm. IR (ATR, selected bands): $\tilde{v}_{max}$ = 3611, 3440, 3258, 3208, 2986, 2859, 2322, 1618, 1549, 1471, 1386, 1314, 1265, 1223, 1156, 1050, 757, 706 cm⁻¹.

H_2L^4·2H_2O: To a solution of L-Pro-MSA (0.72 g, 2.74 mmol) in ethanol (20 mL) was added a solution of N-(naphthalen-1-yl)hydrazine-carbothioamide (0.59 g, 2.74 mmol) in ethanol (5 mL). The reaction mixture was heated to reflux at 85 °C for 30 min. The solvent was evaporated under reduced pressure, and the remaining solution (3 mL) was allowed to stand at 5 °C overnight. The precipitate was filtered off, washed with cold ethanol, and dried in vacuo. Yield: 65.0 % (1.26 g). $C_{25}H_{26}N_4O_3S$·2H_2O (498.60): calcd. C 60.22, H 6.06, N 11.24, S 6.43; found C 60.58, H 5.76, N 11.13, S 6.35. ¹H NMR [500 MHz, $(CD_3)_2SO$, 25 °C]: δ = 11.92 (s, 1 H, C=N-NH), 11.53 (s, 1 H, C_{Ph}-OH), 10.31 (s, 1 H, HN-C_{Ph}), 8.57 (s, 1 H, HC=N), 8.00–7.87 (m, 7H Ar), 7.94 (s, 1 H, C^6H), 6.97 (s, 1 H, C^4H), 4.17 (d, J = 13.36 Hz, 1 H, CH_2), 3.49 (d, J = 13.36 Hz, 1 H, CH_2 peak overlapped with DHO proton signal), 3.37 (m, 1 H, proline peak overlapped with DHO proton signal), 2.94–2.88 (m, 1 H, proline), 2.55–2.35 (m, 1 H, proline), 2.25–2.15 (m, 1 H, proline), 2.20 (s, 3 H, CH_3), 1.95–1.80 (m, 2 H, proline), 1.75–1.65 (m, 1 H, proline) ppm. ¹³C{¹H} NMR [126 MHz, $(CD_3)_2SO$, 25 °C]: δ = 178.07 (C=S), 175.10 (CO_2^-), 154.82 (C_{Ph}-OH), 139.99 (HC=N), 136.33 (C^{Ar}), 134.18 (C^{Ar}), 132.00 (C^4), 131.20 (C^{Ar}), 127.72 (C^{Ar}), 127.01 (C^5), 126.49 (C^{Ar}), 125.92 (C^{Ar}), 123.94 (C^{Ar}), 123.55 (C^3), 120.57 (C^1), 65.66 (CH, proline), 56.46 [CH₂(8)], 53.05 (CH₂, proline), 29.48 (CH₂, proline), 23.47 (CH₂, proline), 20.54 (C^7H_3) ppm. ESI-MS (MeOH, positive): m/z = 485 [H_2L^4 + Na]⁺. ESI-MS (MeOH, negative): m/z = 461 [H_2L^4]⁻. UV/Vis (MeOH): λ (ε, M^{-1} cm⁻¹) = 222 (46523) 340 (18611) 306 (17440) nm. IR (ATR, selected bands): $\tilde{v}_{max}$ = 3612, 3431, 3223, 3018, 2874, 2321, 1622, 1543, 1468, 1390, 1310, 1272, 1159, 1050, 1008, 975, 893, 859, 776, 730, 701 cm⁻¹.

Synthesis of Iron(III) Complexes

[Fe(HL^1)Cl_2] (1): To a solution of H_2L^1·1.5H_2O (0.05 g, 0.14 mmol) in methanol (55 mL) whilst stirring was added a solution of $FeCl_3$·6H_2O (0.05 g, 0.18 mmol) in methanol (2 mL), and the reaction mixture was heated to reflux for 1.5 h. After cooling to room temperature the solvent was evaporated under reduced pressure to ca. 5–10 mL.

X-ray diffraction quality crystals were obtained by vapor diffusion of diethyl ether into the concentrated reaction mixture. These were washed with diethyl ether (5 mL) and dried in vacuo overnight. Yield: 25.0 % (0.02 g). $C_{15}H_{19}Cl_2FeN_4O_3S$ (462.15): calcd. C 38.98, H 4.14, N 12.12, S 6.94; found C 39.20, H 4.19, N 12.24, S 6.73. ESI-MS (MeOH, negative): $m/z = 459$ [Fe(L^1)Cl$_2$]$^-$. UV/Vis (MeOH): λ (ε, M^{-1} cm^{-1}) = 623 (562), 359 (7167), 289 (11433), 252 (12963), 218 (12520) nm. IR (ATR, selected bands): $\tilde{v}_{max}$ = 3368, 3294, 3065, 2979, 2915, 2731, 2693, 1643, 1554, 1398, 1305, 1169, 1049 cm^{-1}.

[Fe(HL^2)Cl$_2$]·1.6H$_2$O (2·1.6H$_2$O): To a solution of **H$_2$L^2**·2H$_2$O (0.24 g, 0.56 mmol) in methanol (70 mL) was added a solution of FeCl$_3$·6H$_2$O (0.21 g, 0.78 mmol) in methanol (6 mL). The reaction mixture was stirred at room temperature for 1 h. The green solution was evaporated under reduced pressure to ca. 10 mL. Crystals of X-ray diffraction quality were obtained after ca. 7 d by vapor diffusion of diethyl ether into the concentrated reaction mixture. These were filtered off, washed with diethyl ether (20 mL), and dried in vacuo overnight. Yield: 32.8 % (0.10 g). $C_{19}H_{25}Cl_2FeN_4O_3S$·1.6H$_2$O (545.07): calcd. C 41.87, H 5.21, N 10.28, S 5.88; found C 41.80, H 4.92, N 9.93, S 5.71. ESI-MS (MeOH, negative): $m/z = 514$ [Fe(L^2)Cl$_2$]$^-$. ESI-MS (MeOH, positive): $m/z = 444$ [Fe(L^2)]$^+$, 480 [Fe(HL^2)Cl]$^+$. UV/Vis (MeOH): λ (ε, M^{-1} cm^{-1}) = 621 (840), 474 sh, 366 (9853), 290 (18981), 267 (16253), 223 (17484) nm. IR (ATR, selected bands): $\tilde{v}_{max}$ = 2973, 2878, 2836, 1724, 1583, 1488, 1445, 1360, 1324, 1233, 1188, 1106, 1041, 993 cm^{-1}.

[Fe(HL^3)(MeOH)Cl$_2$]·0.5H$_2$O (3·0.5H$_2$O): To a solution of **H$_2$L^3**·2H$_2$O (0.14 g, 0.33 mmol) in methanol (70 mL) was added a solution of FeCl$_3$·6H$_2$O (0.12 g, 0.43 mmol) in methanol (6 mL). The reaction mixture was stirred at room temperature for 2 h. The dark brown solution was evaporated under reduced pressure to ca. 10 mL. The crystalline solid was obtained after ca. 10 d by vapor diffusion of diethyl ether (Et$_2$O) into the methanolic solution of the complex. The product was filtered off, washed with diethyl ether (10 mL), and dried in vacuo. Yield: 61.0 % (0.12 g). $C_{22}H_{27}Cl_2FeN_4O_4S$·0.5H$_2$O (579.30): calcd. C 45.61, H 4.87, N 9.67, S 5.54; found C 45.56, H 4.74, N 9.95, S 5.60. ESI-MS (MeOH, positive): $m/z = 466$ [Fe(L^3)]$^+$, 502 [Fe(HL^3)Cl]$^+$, 538 [Fe(H$_2$L^3)Cl$_2$ + H]$^+$. ESI-MS (MeOH, negative): $m/z = 537$ [Fe(L^3)Cl$_2$]$^-$. UV/Vis (MeOH): λ (ε, M^{-1} cm^{-1}) = 547 (1577), 489 (1848), 373 (12522), 316 (14178), 293 sh, 260 sh, 230 (18771), 203 (18908) nm. IR (ATR, selected bands): $\tilde{v}_{max}$ = 3650, 2875, 1632, 1587, 1556, 1492, 1449, 1408, 1345, 1169, 1131, 1059, 1002, 961 cm^{-1}.

[Fe(HL^4)(MeOH)Cl$_2$]·0.5H$_2$O (4·0.5H$_2$O): To a solution of **H$_2$L^4**·2H$_2$O (0.10 g; 2.01 mmol) in ethanol/water (3:2) (75 mL) was added a solution of FeCl$_3$·6H$_2$O (0.067 g, 2.48 mmol) in ethanol (5 mL). The reaction mixture was stirred at room temperature overnight. The solvent was removed under reduced pressure and the residue was dissolved in methanol (5 mL). After addition of Et$_2$O (50 mL) the precipitate was filtered off, washed with Et$_2$O (10 mL), and dried in vacuo overnight. Yield: 59.4 % (0.076 g). $C_{26}H_{29}Cl_2FeN_4O_4S$·0.5H$_2$O (629.36): calcd. C 49.62, H 4.80, N 8.90, S 5.09; found C 49.50, H 4.49, N 8.81, S 4.94. ESI-MS (MeOH, positive): $m/z = 516$ [Fe(L^4)]$^+$. ESI-MS (MeOH, negative): $m/z = 586$ [Fe(L^4)Cl$_2$]$^-$. UV/Vis (MeOH): λ (ε, M^{-1} cm^{-1}) = 551 (1377), 358 (13871), 293 (16636), 249 sh nm. IR (ATR, selected bands): $\tilde{v}_{max}$ = 3655, 2967, 2920, 1730, 1560, 1447, 1397, 1319, 1265, 1232, 1169, 1070, 1009, 924 cm^{-1}.

[Fe(HL^4)(DMF)Cl$_2$]·0.5Et$_2$O·H$_2$O (4′·0.5Et$_2$O·H$_2$O): Complex **4** (7 mg) was dissolved in dimethylformamide (DMF) (0.6 mL). Vapor diffusion of Et$_2$O into the DMF solution of **4** yielded crystals of **4′** with X-ray diffraction quality. Yield: 75.8 % (5.5 mg). $C_{28}H_{32}Cl_2FeN_5O_4S$·0.5Et$_2$O·H$_2$O (716.48): C 50.29, H 5.49, N 9.77, S

4.48; found C 50.04, H 5.12, N 9.82, S 4.20. ESI-MS (MeOH, positive): $m/z = 516$ [Fe(L^4)]$^+$, 589 [Fe(HL^4)Cl$_2$ + H]$^+$. ESI-MS (MeOH, negative): $m/z = 586$ [Fe(L^4)Cl$_2$]$^-$, 550 [Fe(HL^4)Cl]$^-$, 459 (HL$^-$). UV/Vis (DMF): λ (ε, M^{-1} cm^{-1}) = 548 sh, 368 (12066), 307 (13043) nm. IR (ATR, selected bands): $\tilde{v}_{max}$ = 3060, 2966, 2926, 2858, 2654, 2326, 1987, 1672, 1638, 1593, 1565, 1459, 1384, 1322, 1259, 1227, 1171, 1117, 1067, 1007, 971, 875, 828, 771, 679, 605 cm^{-1}.

Crystallographic Structure Determination: X-ray diffraction measurements of complexes **1**–**3** were performed with a Bruker D8 Venture (or Bruker X8 APEXII CCD) and that of complex **4′** with a STOE StadiVari diffractometer [detector Dectris Pilatus 300 K, microfocus source Incoatec IμS Cu (Cu-K_α, $\lambda = 1.54184$ Å) at 100 K]. The Bruker diffractometer was equipped with an Oxford Cryosystem nitrogen gas open-flow cooler and Stoe StadiVari with a nitrogen gas open-flow Cobra from Oxford Cryosystem. The proline carbon atom C12B and pyrrolidine carbon atoms C17B and C18B in one of the two crystallographically independent molecules in **2** were disordered over two positions with site occupation factors (s.o.f.) 0.70 to 0.30 and 0.60 to 0.40, respectively. The disorder involving the proline carbon atoms C12B and C13B and the coordinated methanol carbon atom C22B in **3** was also resolved over two positions with s.o.f. 0.75 to 0.25, while that of carbon atom C9 in **4′** with s.o.f. 0.60 to 0.40. In all cases the disorder was resolved by using SADI and EADP restraints implemented in SHELXL. Some electron density in the crystal structure of **2** was found in special positions and these were modelled as partly occupied with diethyl ether and water molecules. The site population was obtained from thermal parameters upon refinement with further constraints to the composition **2**·0.2CH$_3$OH·0.125Et$_2$O·0.063H$_2$O. The software programs used for structure solution were SHELXS-97[39] and X-Area STOE,[40] for structure refinement SHELXL-97[39] and XD2006, respectively, and for molecular diagrams ORTEP-3.[41]

CCDC 1557747 (for **1**), 1557748 (for **2**), 1557749 (for **3**), and 1557750 (for **4′**) contain the supplementary crystallographic data for this paper. These data can be obtained free of charge from The Cambridge Crystallographic Data Centre.

Physical Measurements: Elemental analysis of all compounds was performed with a Perkin–Elmer 2400 CHN Elemental Analyser (Perkin–Elmer, Waltham, MA) at the Microanalytical Laboratory of the University of Vienna. Microanalytical data are within ±0.4 % of the calculated values. Electrospray ionisation mass spectrometry measurements were carried out with a Bruker Esquire 3000 instrument (Bruker Daltonic, Bremen, Germany) at the Mass Spectrometry Centre of the Faculty of Chemistry (University of Vienna). UV/Vis spectra were measured with a Perkin–Elmer Lambda 650 spectrophotometer. The samples were prepared by dissolving the compounds in MeOH, DMF, or solvent mixture MeOH/H$_2$O (1:1) before measurement (900–210 nm). Infrared spectra were recorded with a Perkin–Elmer FTIR 2000 instrument (400–400 cm^{-1}) by using the ATR unit or a Bruker Vertex 70 FTIR spectrometer. NMR spectra were acquired with a Bruker Avance III 500 MHz FT-NMR spectrometer by using (CD$_3$)$_2$SO as a solvent. Magnetic measurements were carried out on microcrystalline samples **2** and **4** with a Quantum Design SQUID magnetometer (MPMS-XL) at 0.1 T in the temperature range 2–300 K. Data were corrected for the contribution of the sample holder and diamagnetism of the samples estimated from Pascal's constants.[42]

Electrochemistry Measurements: For cyclic voltammetry experiments commercially available acetonitrile (MeCN) Secco Solv (dried, max. 0.005 % H$_2$O) from Merck, and ferrocene (Fc) purchased from Sigma Aldrich were used without further purification. Tetrabutyl-ammonium hexafluorophosphate (nBu$_4$NPF$_6$) of purissimum quality

(Fluka) was dried under reduced pressure at 70 °C for 24 h. Cyclic voltammograms of the complexes in MeCN (1 mM) containing $n\mathrm{Bu_4NPF_6}$ (0.1 M) as the supporting electrolyte were measured by using a one-compartment electrochemical cell with platinum wires as the working and counter electrodes and a silver wire as the pseudoreference electrode. All electrochemical measurements were performed under a nitrogen atmosphere. Cyclic voltammograms were measured with a HEKA PG 390 potentiostat at room temperature. DigiElch Professional software from Gamry Instruments (USA), version DigiElch8, was used for digital simulations of cyclic voltammograms.

Cytotoxicity Assay

Cell Lines and Culture Conditions: Human cervical carcinoma (HeLa), human melanoma (FemX), human alveolar basal adenocarcinoma (A549), human breast cancer (MDA-MB-453), colon cancer cell line (LS-174), murine transformed endothelial cell line (MS1), and normal lung fetal fibroblast cell line (MRC-5) were maintained as monolayer culture in the Roswell Park Memorial Institute (RPMI) 1640 nutrient medium (Sigma Chemicals Co, USA). RPMI 1640 nutrient medium was prepared in sterile ionized water, supplemented with penicillin (192 IU mL^{-1}), streptomycin (200 mg mL^{-1}), 4-(2-hydroxyethyl)piperazine-1-ethanesulfonic acid (HEPES) (25 mM), L-glutamine (3 mM), and of heat-inactivated fetal calf serum (FCS; 10 %, pH 7.2). The cells were grown at 37 °C in CO_2 (5 %) and humidified in air atmosphere, by twice weekly subculture.

MTT Assay: Antiproliferative activity of the compounds was determined by using 3-(4,5-dimethylthiazol-yl)-2,5-diphenyltetrazolium bromide (MTT, Sigma Aldrich) assay.[43] Cells were seeded into 96-well cell culture plates (Thermo Scientific Nunc) in an appropriate density for each cell line. After 24 h of growth, cells were exposed to the serial dilutions of the tested compounds. The compounds were dissolved in minimum amount of dimethyl sulfoxide (DMSO) and afterwards diluted with nutrient medium to the desired final concentrations (in the range up to 300 μM). The amount of DMSO in the prepared solutions was ≤ 1 %. Each concentration was tested in triplicate. After an incubation period of 48 h, MTT solutions (20 μL, 5 mg mL^{-1} in phosphate buffer solution, pH 7.2) were added to each well. Samples were incubated at 37 °C with CO_2 (5 %) in a humidified atmosphere for 4 h. Formazan crystals were dissolved in 100 μL of 10 % sodium dodecyl sulfate (SDS). Absorbance values were recorded after 24 h with an ELISA reader (ThermoLabsystem Multiskan EX 200–240 V) at the wavelength of 570 nm. The IC$_{50}$ values, defined as the concentrations of the compound causing 50 % cell growth inhibition, were estimated from the dose–response curves.

Notes

The authors declare no competing financial interest.

[1] a) D. X. West, S. B. Padhye, P. B. Sonawane, *Struct. Bonding (Berlin)* **1991**, *76*, 1–50; b) T. S. Lobana, R. Sharma, G. Bawa, S. Khanna, *Coord. Chem. Rev.* **2009**, *253*, 977–1055; c) T. S. Lobana, *RSC Adv.* **2015**, *5*, 37231–37274.

[2] Y. Yu, D. S. Kalinowski, Z. Kovacevic, A. R. Siafakas, P. J. Jansson, C. Stefani, D. B. Lovejoy, P. C. Sharpe, P. V. Bernhardt, D. R. Richardson, *J. Med. Chem.* **2009**, *52*, 5271–5294.

[3] H. Beraldo, D. Gambino, *Mini-Rev. Med. Chem.* **2004**, *4*, 31–39.

[4] D. Hamre, J. Bernstein, R. Donvick, *Proc. Soc. Exp. Biol. Med.* **1950**, *73*, 275–278.

[5] R. C. DeConti, B. R. Toftness, K. C. Agrawal, R. Tomchick, J. A. R. Mead, J. R. Bertino, A. C. Sartorelli, W. A. Creasey, *Cancer Res.* **1972**, *32*, 1455–1462.

[6] I. H. Krakoff, E. Etcubanas, C. Tan, K. Mayer, V. Bethune, J. H. Burchenal, *Cancer Chemother. Rep.* **1974**, *58*, 207–212.

[7] M.-C. Liu, T.-S. Lin, A. C. Sartorelli, *J. Med. Chem.* **1992**, *35*, 3672–3677.

[8] C. Stefani, P. J. Jansson, E. Gutierrez, P. V. Bernhardt, D. Richardson, *J. Med. Chem.* **2013**, *56*, 357–370; and references cited therein.

[9] P. Nordlund, P. Reichard, *Annu. Rev. Biochem.* **2006**, *75*, 681–706.

[10] B. M. Zeglis, V. Divilov, J. S. Lewis, *J. Med. Chem.* **2011**, *54*, 2391–2398.

[11] J. Yuan, D. B. Lovejoy, D. R. Richardson, *Blood* **2004**, *104*, 1450–1458.

[12] C. P. Wu, S. Shukla, A. M. Calcagno, M. D. Hall, M. M. Gottesman, S. V. Ambudkar, *Mol. Cancer Ther.* **2007**, *6*, 3287–3296.

[13] S. Sahni, D.-H. Bae, D. J. R. Lane, Z. Kovacevic, D. S. Kalinowski, P. J. Jansson, D. R. Richardson, *J. Biol. Chem.* **2014**, *289*, 9692–9709.

[14] P. J. Jansson, D. S. Kalinowski, D. J. Lane, Z. Kovacevic, N. A. Seebacher, L. Fouani, S. Sahni, A. M. Merlot, D. R. Richardson, *Pharmacol. Res.* **2015**, *100*, 255–260.

[15] I. Đilovic, M. Rubcic, V. Vrdoljak, S. K. Pavelic, M. Kralj, I. Piantanida, M. Cindric, *Bioorg. Med. Chem.* **2008**, *16*, 5189–5198.

[16] C. R. Kowol, R. Trondl, P. Heffeter, V. B. Arion, M. A. Jakupec, A. Roller, M. Galanski, W. Berger, B. K. Keppler, *J. Med. Chem.* **2009**, *52*, 5032–5043.

[17] C. Stefani, G. Punnia-Moorthy, D. B. Lovejoy, P. J. Jansson, D. S. Kalinowski, P. C. Sharpe, P. V. Bernhardt, D. Richardson, *J. Med. Chem.* **2011**, *54*, 6936–6948.

[18] M. N. M. Milunovic, E. A. Enyedy, N. V. Nagy, T. Kiss, R. Trondl, M. A. Jakupec, B. K. Keppler, R. Krachler, G. Novitchi, V. B. Arion, *Inorg. Chem.* **2012**, *51*, 9309–9321.

[19] https://doi.org/ttps://clinicaltrials.gov/ct2/show/NCT02433626, accessed on 24/06/2017.

[20] K. Y. Salim, S. M. Vareki, W. R. Danter, J. Koropatnick, *Oncotarget* **2016**, *7*, 41363–41379.

[21] F. Bacher, E. A. Enyedy, N. V. Nagy, A. Rockenbauer, G. M. Bognar, R. Trondl, M. S. Novak, E. Klapproth, T. Kiss, V. B. Arion, *Inorg. Chem.* **2013**, *52*, 8895–8908.

[22] S. Ishida, P. Andreux, C. Poitry-Yamate, J. Auwerx, D. Hanahan, *Proc. Natl. Acad. Sci. USA* **2013**, *110*, 19507–19512.

[23] Y. Gou, J. Wang, S. Chen, Z. Zhang, Y. Zhang, W. Zhang, F. Yang, *Eur. J. Med. Chem.* **2016**, *123*, 354–364.

[24] J. Qi, Y. Gou, Y. Zhang, K. Yang, S. Chen, L. Liu, X. Wu, T. Wang, W. Zhang, F. Yang, *J. Med. Chem.* **2016**, *59*, 7497–7511.

[25] A. Popovic-Bijelic, C. R. Kowol, M. E. S. Lind, J. Luo, F. Himo, E. A. Enyedy, V. B. Arion, A. Gräslund, *J. Inorg. Biochem.* **2011**, *105*, 1422–1431.

[26] J. M. Phang, W. Liu, C. N. Hancock, J. W. Fisher, *Curr. Opin. Clin. Nutr. Metab. Care* **2015**, *18*, 71–77.

[27] O. J. Patino, L. E. Cuca, *Phytochem. Lett.* **2011**, *4*, 22–25.

[28] A. Dobrova, S. Platzer, F. Bacher, M. N. M. Milunovic, A. Dobrov, G. Spengler, E. A. Enyedy, G. Novitchi, V. B. Arion, *Dalton Trans.* **2016**, *45*, 13427–13439.

[29] A. W. Addison, T. N. Rao, J. Reedijk, J. van Rijn, G. C, *J. Chem. Soc., Dalton Trans.* **1984**, 1349–1356.

ChemPubSoc
Europe

EurJIC
European Journal
of Inorganic Chemistry

Full Paper

[30] D. Carmona, M. P. Lamata, F. Viguri, I. Dobrinovich, F. L. Lahoz, L. A. Oro, *Adv. Synth. Catal.* **2002**, *344*, 499–502.

[31] E. A. Enyedy, M. F. Primik, C. R. Kowol, V. B. Arion, T. Kiss, B. K. Keppler, *Dalton Trans.* **2011**, *40*, 5895–5905.

[32] O. Kahn, *Molecular Magnetism*, VCH Publishers, New York, Weinheim, Cambridge, **1993**.

[33] D. Gatteschi, R. Sessoli, J. Villain, *Molecular Nanomagnets*, Oxford University Press, Oxford, **2006**.

[34] V. V. Pavlishchuk, A. W. Addison, *Inorg. Chim. Acta* **2000**, *298*, 97–102.

[35] D. R. Richardson, P. C. Sharpe, D. B. Lovejoy, D. Senaratne, D. S. Kalinowski, M. Islam, P. V. Bernhardt, *J. Med. Chem.* **2006**, *49*, 6510–6521.

[36] D. S. Kalinowski, P. C. Sharpe, P. V. Bernhardt, D. R. Richardson, *J. Med. Chem.* **2007**, *50*, 6212–6225.

[37] F. Bacher, O. Domotor, M. Kaltenbrunner, M. Mojovic, A. Popovic-Bijelic, A. Graslund, A. Ozarowski, L. Filipovic, S. Radulovic, E. A. Enyedy, V. B. Arion, *Inorg. Chem.* **2014**, *53*, 12595–12609.

[38] A. Basu, G. Das, *Dalton Trans.* **2011**, *40*, 2837–2843.

[39] G. M. Sheldrick, *Acta Crystallogr., Sect. A: Fundam. Crystallogr.* **2008**, *64*, 112–122.

[40] STOE & Cie GmbH (**2016**), *X-Area 1.76*, software package for collecting single-crystal data on STOE area-detector diffractometers, for image processing, scaling reflection intensities and for outlier rejection; Darmstadt, Germany.

[41] M. N. Burnett, G. K. Johnson, *ORTEPIII, Report ORNL-5138*, Oak Ridge National Laboratory, Oak Ridge, TN, **1996**.

[42] G. A. Bain, J. F. Berry, *J. Chem. Educ.* **2008**, *85*, 532–536.

[43] R. Supino, *In vitro Toxicity Testing Protocols*, Springer, New York, **1995**, p. 37–149.